Effect of Reactive Channel Functional Groups and Nanoporosity of Nanoscale Mesoporous Silica on Properties of Polyimide Composite

Chi-Feng Cheng,* Hsu-Hsuan Cheng, Po-Wen Cheng, and Yueh-Ju Lee

Department of Chemistry, Center of Nanotechnology and R&D Center for Membrance and Technology, Chung Yuan Christian University, 200, Chung Pei Rd., Chung Li, Taiwan 32023, R.O.C.

Received May 3, 2006; Revised Manuscript Received August 22, 2006

ABSTRACT: Novel covalently bonded nanoscale mesoporous silica (NMS)/polyimide (ODPA−BAPP) nanocomposites were synthesized through the bridge 3-aminopropyltrimethoxysilane. Abundant reactive amino functional groups inside the mesopore channels of NMS can interconnect with numerous polyimide main chains, forming multilinked and complex NMS/PI networks. These multilinkages, NMS inherent nanoporosity, and the uniform dispersion of NMS in polyimide significantly improve thermal stability, mechanical properties, elongation, moisture absorption, and dielectric constant of these novel materials over those of neat polyimide. For instance, the storage modulus is increased by 160%, the decomposition temperature by 35.7 °C, and the glass transition temperature by 14.5 °C. The maximum elongation increases by 66%, hardly observed in other polyimide nanocomposites, probably because the covalent bond and NMS nanopore can absorb more energy than pristine poyimide before failure. The nanoporosity of the core of the NH_2-NMS material within the nanocomposite film is most likely responsible for the decrease of dielectric constant by 10%.

Introduction

Organic−inorganic hybrid materials are recognized as a new class of advanced materials because they can be synthesized or processed using versatile approaches and own tunable properties.[1,2] Inorganic materials, such as silica, exhibit excellent thermal stability and hardness. The incorporation of well-dispersed (preferably on the nanometer scale) silica particles into polymer matrices has been shown to be an extremely effective approach to improve the thermal and mechanical properties of polymers.[3,4]

Among aromatic polymer materials, polyimides exhibit outstanding thermal and mechanical properties and lower dielectric constants than other polymers. Hence, they are widely applied in the space and electrical industries and are well-known as important high-performance polymers.[5−7] Various reports have focused on sol−gel processing, intercalation, and in-situ polymerization **(**with inorganic particles such as silica and alumina) employed to prepare polyimide/inorganic nanocomposites. These hybrid materials reported in the literature may have better thermal stability and mechanical strength than their parent polyimides.[8−17] The key challenge for the preparation of the hybrid materials is to avoid phase separation between the organic and inorganic moieties. The phase behavior is related to the interaction between the inorganic segment and the organic network. Hydrogen bonding or covalent bonding typically prevents phase separation.[18,19] Although several studies have addressed the thermal and mechanical characteristic of polyimide/silica hybrid, very little attention has been paid to its dielectric constant, which dielectric constant monotonically increases with the content of silica particles.[20,21] Recently, a series of polyimide hybrids based on several types of polyhedral oligomeric silsesquioxane (POSS) have been prepared and investigated.[22−32] POSS bound to polyimide matrix has been shown to reduce the dielectric constant without significantly degrading the mechanical and thermal properties of polyimide because the porosity is controllable and silica is stable.[23−25,28,29] Furthermore, the incorporation of POSS into polyimide in some cases slightly enhanced thermal and mechanical properties[30,32,33] and reduced the uptake of water.[34] However, POSS may be too expensive to apply to the electronics industry.

Recently, the nanoscale silica-based mesoporous materials have become known for their potentially useful catalytic, magnetic, optical, and semiconducting properties, which are exploited in technological and biomedical applications.[35−37] Nanoscale mesoporous silica (NMS) is a good candidate for the inorganic component of the polyimide nanocomposite because of its excellent thermal and mechanical stability and inherent air void inside the nanochannels. Moreover, it is less expensive than POSS. Nanosized mesoporous silica is better able to be dispersed evenly in the polyimide matrix on nanoscale through moderate hydrogen bonding or covalent bonding than on microscale. Since abundant silanol groups inside the mesopore channel and on the particle surface can bond with silane attaching different functional groups, functionalized nanoscale mesoporous silica (NMS) can form covalent bonds with organic monomers or polymer. Their incorporation into some polymers may improve the thermal stability, the mechanical properties, and the dielectric constant. The main reason, unique to this material, is related to the nanoporosity in NMS and nanosize of NMS. Polymer chains not only covalently bond with many reactive channel functional groups of NMS but also exert the van der Waals forces on channel surface molecules due to the polymer intrusion into NMS nanopores.

This work reports the homogeneous dispersion of nanoscale mesoporous silica into polyimide matrix to form novel NMS/polyimide nanocomposites via covalent bonding. Novel NMS/PI organic−inorganic hybrid materials were studied based on organo-soluble polyimide from BAPP (2,2-bis[4-(4-aminophenoxy)phenyl]propane) and ODPA (4,4′-oxydiphthalic anhydride) by in-situ polymerization. The amino-functionalized NMS was employed as an inorganic moiety to form the intrachain covalent bonds and interchain hydrogen bonds with polyimide. The nanoscale amino-functionalized mesoporous silica was further

* To whom correspondence should be addressed: Ph +886-3-2653338; Fax +886-3-2653399; e-mail chifeng@cycu.edu.tw.

10.1021/ma060990u CCC: $33.50
Published on Web 09/28/2006

Scheme 1. Synthesis of ODPA-NH_2-NMS and NMS/PI Nanocomposite

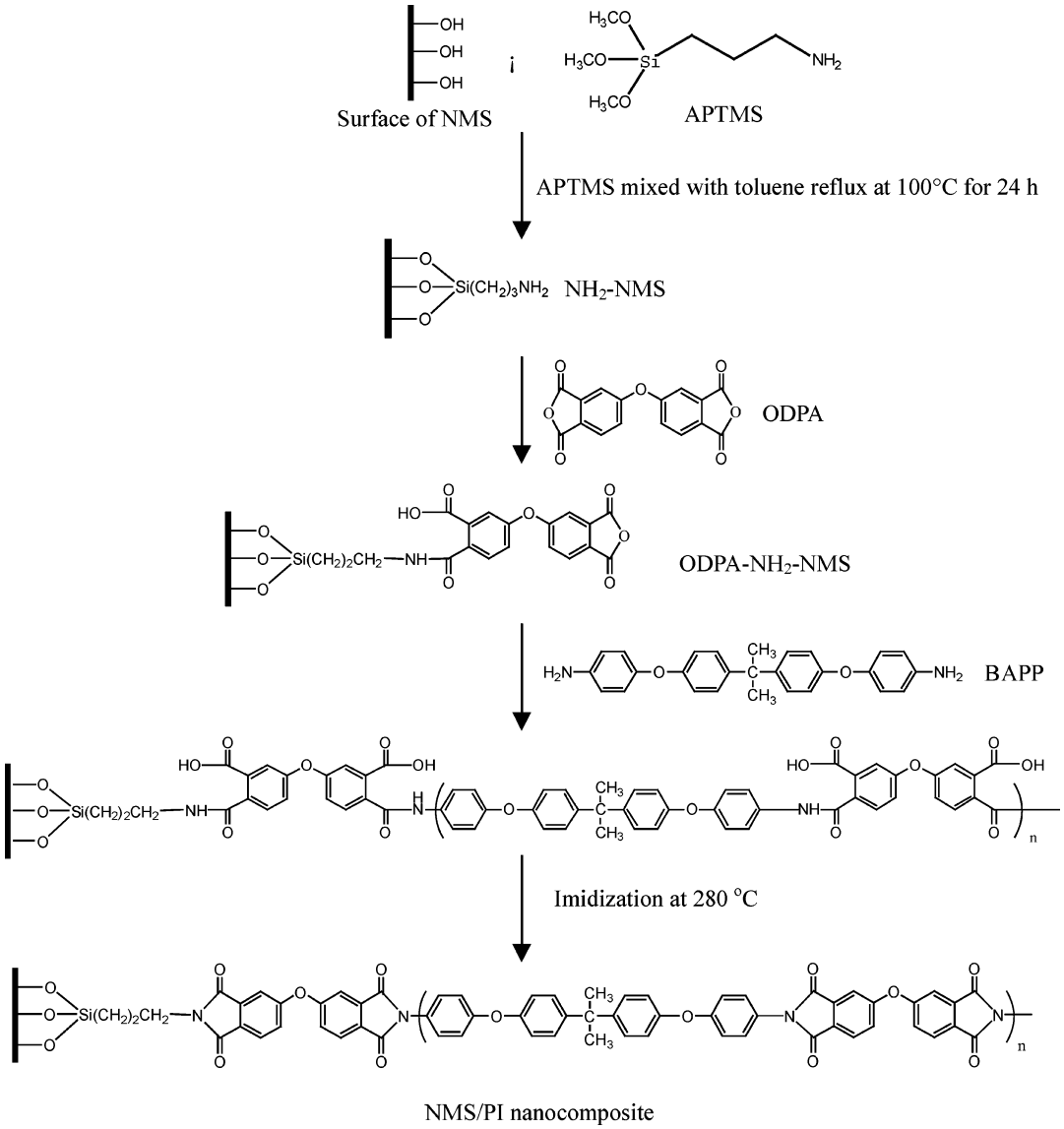

functionalized with a special anhydride end group that is structurally identical to the anhydride connected to the polymer. Numerous reactive amino functional groups inside the mesopore channels of NMS can interconnect with several polyimide main chains, forming multilinked and complex NMS/PI networks. The bonding between polyimide main chains and reactive amino functional groups inside NMS channel significantly improves tensile strength, modulus, thermal properties, dielectric constant, and elongation of this novel composite.

Experimental Section

Materials. Tetramethylammonium hydroxide (TMAOH, 25 wt %) and fumed silica (99.8%) were purchased from Aldrich and Sigma, respectively. Cetyltrimethylammonium bromide (CTABr, >99%) and 3-aminopropyltrimethoxysilane (APTMS, 99%) were obtained from Acros. 4,4′-Oxydiphthalic anhydride (ODPA, 98%) and 2,2-bis[4-(4-aminophenoxy)phenyl]propane (BAPP, 98%) used as polyimide monomers were obtained from Chriskev. *N*-Methylpyrrolidinone (NMP, 99.5%) was purchased from Tedia.

Synthesis of Nanoscale Mesoporous Silica.[37] Nanoscale mesoporous silica (denoted as NMS) was prepared as follows: 7.72 g of TMAOH and 10.98 g of CTABr were added to a beaker that contained 74.6 g of deionized water with stirring at room temperature. Fumed silica (6.7 g) was added to the homogeneous solution, which was stirred to form a reactive gel at 30 °C for 1 h. The resultant gels were loaded into double-walled digestion vessels and irradiated with 1000 W of microwaves to the desired temperature, 180 °C, for 5 min. After crystallization, these nanoscale mesoporous silica materials were filtered off, washed with distilled water, dried in air at 80 °C, and calcined at 550 °C for 6 h. The molar ratio of SiO_2:TMAOH:CTABr:H_2O was 1:0.19:0.27:40 in the final gel mixture. Microwave-hydrothermal synthesis was performed using a MARS5 (CEM Corp.) microwave digestion system with a controllable temperature and pressure unit.

Aminopropyl Functionalization of Nanoscale Mesoporous Silica (NH_2-NMS). The surface of nanoscale mesoporous silica was modified using APTMS shown as Scheme 1. This molecule contains an NH_2 group, a stable propyl spacer, and a hydrolyzable $Si(OMe)_3$ moiety. In a typical experiment, nanoscale mesoporous silica (1 g) and APTMS (2 g) were added into a round-bottomed flask with toluene (10 mL). This mixture was stirred under reflux at 100 °C for 24 h. These materials were filtered, repeatedly washed with toluene solution, and dried in air at 90 °C. The mass of final product was about 1.3 g, which consists of 1.0 g of NMS and 0.3 g of APTMS.

In-Situ Polymerization of NH_2-NMS/PI Nanocomposite Films by Thermal Imidization. A typical procedure for preparing the NMS/polyimide by thermal imidization (Scheme 1) is as follows. ODPA (1.395 g, 4.5 mmol) was put into a three-neck flask that

contained 29.0 g of dry NMP at room temperature with continuous stirring for 12 h under nitrogen gas purge. An appropriate amount of NH_2-NMS, i.e., 1, 3, 5, 7, or 10 wt % of polyimide, was introduced into the flask under stirring for 24 h at room temperature. Then, 1.838 g (4.5 mmol) of BAPP was added to the above solution with vigorous stirring for 24 h at room temperature to form a viscous and homogeneous polyamic acid (PAA) solution. The obtained solution of the NMS/polyamic acid was spread onto a glass plate, which was placed in an oven at 80 °C for 1 h to remove some of the solvent. The semidried PAA film was heated for 1 h at each of 120, 130, 150, 180, and 210 °C sequentially and then for 0.5 h at each 250 and 280 °C. A flexible NMS/polyimide film was self-stripped from the glass surface by soaking in water.

Characterization. X-ray powder diffraction (XRD) patterns were obtained using a Rigaku X-ray diffractometer with Cu Kα radiation (λ = 1.5418 Å) at 35 kV and 25 mA. The nanoscale silica mesoporous samples were recorded with a step size of 0.02°and a step time of 1 s over the angular range $1° < 2\theta < 6°$. N_2 adsorption/desorption isotherms were obtained at −196 °C. The specific surface area, A_{BET}, was determined from the linear part of the BET plot (P/P_0 = 0.05−0.30) using a Micrometrics ASAP 2010 system at −196 °C. The pore size was obtained from the maximum of the pore size distribution using the BJH model applied to adsorption data. NMS and NH_2-NMS were degassed at 350 and 110 °C, respectively, under a pressure of 10^{-3} Torr for at least 8 h. Elemental analyses (EA) were performed on a Heraeus CHNS elemental analyzer. MAS NMR spectra were recorded at 9.4 T using a Bruker Avance 400 spectrometer, with zirconia rotors with diameter of 4 mm spun at 5 kHz. ^{13}C spectra were obtained at 100.6 MHz using the cross-polarization (CP) technique and TMS as a reference. Infrared spectra of KBr disks were recorded on a JASCO FT/IR-460 plus spectrometer. The samples for transmission electron microscopy (TEM) were initially prepared by putting the polyimide membranes into epoxy resin capsules and then curing the epoxy resin at 80 °C for 20 h in a vacuum oven. Then, the cured epoxy resin, containing the polyimide materials, was embedded and sectioned in a Leica Ultracut UCT at room temperature into 60 nm thick slices, and these thin slices were placed on a mesh 200 carbon-coated copper grid for TEM observation. TEM microphotographs were taken using a JEOL-JEM 2010 instrument operated at 200 keV. The thermal stabilities of the neat polyimide and the polyimide nanocomposites were characterized by thermal gravimetric analysis (TGA) and differential scanning calorimetry (DSC). TGA of the polyimide films was conducted using a Du Pont TA Instruments TGA Q 50 at a heating rate of 20 °C/min from 50 to 900 °C in an atmosphere of nitrogen. DSC was performed using a Du Pont TA Instruments DSC Q 10 from 35 to 400 °C in flow nitrogen at the programmed heating rate of 10 °C /min. Dynamic mechanical analysis (DMA) measurements were made using a Du Pont TA Instruments DMA Q 800 at a heating rate of 3 °C/min from 35 to 350 °C and a frequency of 1 Hz. The stress/strain behaviors of all samples under uniaxial tension (1 N/min) were measured using a TA model Q 800. Free-standing films of the samples, used to make these measurements, were 4 mm wide and 30 mm long. Dielectric properties were measured as a function of frequency and temperature with a HP (Hewlett-Packard) 4192A impedance gain phase analyzer. The samples whose water uptake was measured were dried at 100 °C for 24 h in vacuo and then put in a sealed container at 30 °C at a relative humidity of 100%.

Results and Discussion

Novel NMS/PI organic−inorganic hybrid materials based on organo-soluble polyimide from BAPP and ODPA were studied by in-situ polymerization. Scheme 1 presents the reaction path of this nanocomposite synthesis. Nanoscale mesoporous silica with an amino end group (NH_2-NMS) was obtained initially by reacting NMS with APTMS (3-aminopropyltrimethoxysilane). A model compound precursor (ODPA-NH_2-NMS) for the covalently bonded NMS/polyimide nanocomposite was prepared by reacting NH_2-NMS with anhydride to form anhydride-amino-NMS. In particular, one functionalized NMS particle has many anhydride functional end groups inside its mesoporous channel and on the particle surface; these end groups readily react with BAPP and ODPA, forming NMS-bonded PAA in solution. After imidization at 280 °C, a polyimide nanocomposite formed.

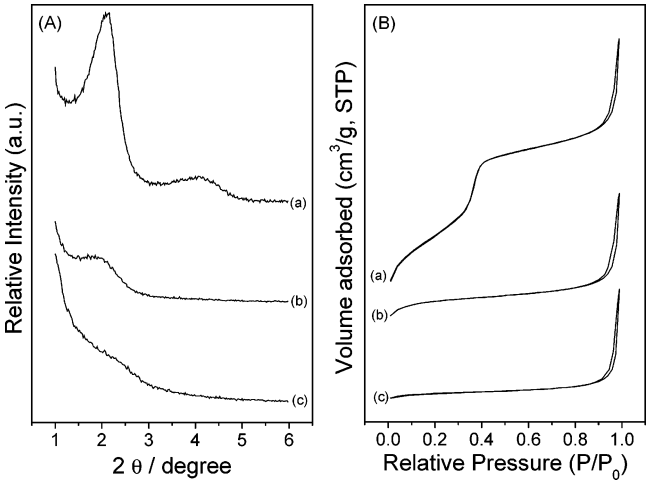

Figure 1. (A) XRD patterns and (B) nitrogen sorption isotherms at −196 °C of (a) NMS, (b) NH_2-NMS, and (c) ODPA-NH_2-NMS materials.

Chemical Modification and Mesostructure of Nanoscale Mesoporous Silica. Figure 1A displays small-angle X-ray diffraction patterns of different NMS materials.[37] These materials exhibit one broad peak in the low-angle range, which is usually associated with the (100) reflection when a hexagonal cell is assumed. The concept of the microwave hydrothermal synthesis of nanoscale mesoporous materials has been discussed elsewhere.[37] The broad peak is attributed to wormlike pores and nanoscale particles. XRD diffraction patterns of both the NH_2-NMS and ODPA-NH_2-NMS extracted samples are similar to that of pure siliceous NMS. However, the peak intensity of the (100) diffraction declines and become less well resolved after the aminopropyl functionalization of NMS materials or further immobilization of anhydride on NH_2-NMS materials. Figure 1B displays the N_2 adsorption/desorption isotherms of different NMS materials. The N_2 adsorption−desorptiom isotherms of these samples exhibit two capillary adsorptions at partial pressures (P/P_0) of 0.3−0.4 and >0.9. The former capillary adsorption at a partial pressure (P/P_0) of 0.3−0.4 is attributed to the typical mesopore. Other capillary adsorption at P/P_0 > 0.9 is associated with the textural mesoporosity, which results from the interparticle space in the aggregation of nanoparticles. NMS has a pore diameter of 2.70 nm, but the pore diameters of NH_2-NMS and ODPA-NH_2-NMS are below the instrumental detection limit of 1.7 nm. NH_2-NMS has a lower total pore volume of 0.59 cm^3/g than its parent NMS (1.16 cm^3/g). ODPA-NH_2-NMS has the pore volume of 0.21 cm^3/g. Nanopores of functionalized nanoscale mesoporous silica were partially filled with ODPA-NH_2 and readily formed covalent bonds with PAA oligomers. Notably, the surface area of NMS declines from 944 m^2/g to 275 and 93 m^2/g after the pore surface modification using APTMS and ODPA, respectively. The surface area, pore size, and pore volume of the functionalized NMS are lower than the corresponding values of the parent NMS. This reveals that the bonding between silanol groups inside the pore channels and silanes causes the partial blockage of the pore channel by APTMS and APTMS−ODPA bonding molecules.

The SEM image shows that the particle size of most NMS is less than 60 nm, and these nanoparticles have an irregular

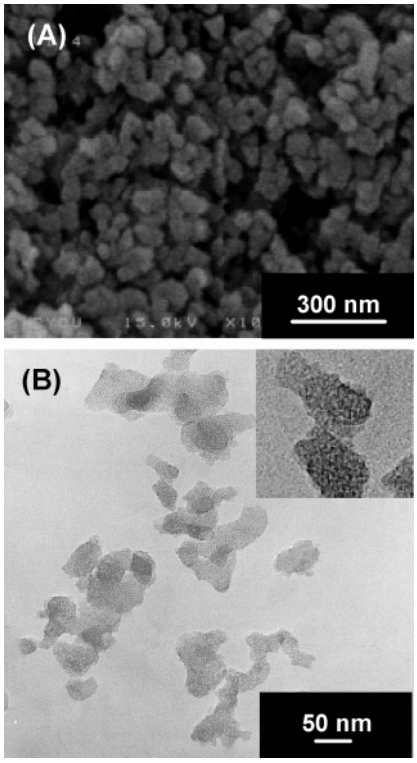

Figure 2. (A) SEM and (B) TEM micrographs of NMS materials. Enlarged NMS is shown in the inset.

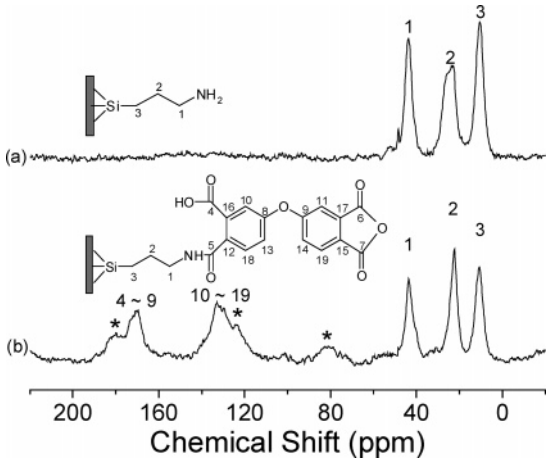

Figure 3. ^{13}C NMR spectrum of (a) NH_2-NMS and (b) ODPA-NH_2-NMS materials. Asterisks denote spinning sidebands.

particle morphology, as displayed in Figure 2A. Careful observation of the high-resolution TEM image in Figure 2B indicates that most nanoparticles are smaller than 60 nm and have the wormhole-like mesostructures with a pore size of 2.5−3.0 nm, which range is consistent with the results of N_2 adsorption/desorption.

The soild-state ^{13}C NMR and FTIR spectra of NH_2-NMS and ODPA-NH_2-NMS can show the chemical structure of these materials obtained by grafting the APTMS and OPDA onto NMS as shown in Figures 3 and 4, respectively.

The three peaks with nearly equal intensity at around 10, 22, and 44 ppm in Figure 3a are related to three different kinds of C atoms for the APTMS group, confirming the existence of APTMS bonded to NMS surface. The ^{13}C CPMAS NMR spectrum of ODPA-NH_2-NMS in Figure 3b displays two more broad peaks at 110−150 and 160−190 ppm, which are associated with chemical structures of benzene and the C═O

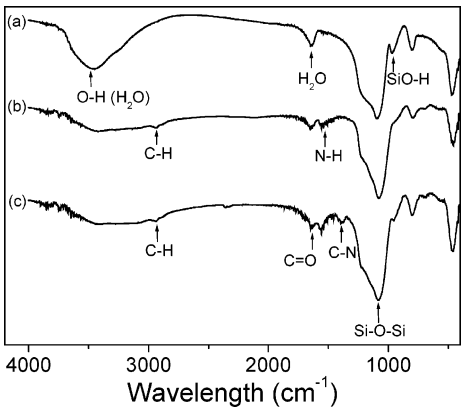

Figure 4. FTIR spectra of (a) NMS, (b) NH_2-NMS, and (c) ODPA-NH_2-NMS materials.

or C−O−C groups, respectively, of immobilized anhydride of ODPA on NH_2-NMS materials. Parts a, b, and c of Figure 4 display FTIR spectra of pure siliceous NMS, NH_2-NMS, and ODPA-NH_2-NMS materials, respectively. For NH_2-NMS and ODPA-NH_2-NMS, the bands at 3460 and 1638 cm^{-1} are attributed to the stretching (3460 cm^{-1}) and bending (1638 cm^{-1}) vibrations of water molecules adsorbed on the surface of the mesoporous materials.[38] The intensity of the ≡Si−OH bending vibration absorption band for NMS at 967 cm^{-1} markedly decreases after the reaction with APTMS silane. Additionally, one new band appears at 1540 cm^{-1} due to N−H bending vibration, and another new band appears between 2800 and 3000 cm^{-1} associated with the C−H stretching vibration in the NH_2-NMS. These findings indicate the bonding between APTMS and surface ≡SiO−H groups on NMS. After NH_2-NMS further reacted with ODPA dianhydride, a new band at 1425 cm^{-1} appeared, associated with the C−N stretching vibration, suggesting the bonding between ODPA and NH_2-NMS.

Element analysis results of NMS, NH_2-NMS, and ODPA-NH_2-NMS are shown in Table 1. NH_2-NMS has a higher carbon content (8.5 wt %) than the parent NMS. Additional ODPA bonding with NH_2-NMS increases the carbon content to 14.3 wt %. Accordingly, these element analyses indicate the incorporation of aminopropyl followed by anhydride group not only on the particle surface but also into the channel surface of nanoscale mesoporous silica.

Characterization and Properties of Nanocomposite Films. *Morphology of Polyimide Nanocomposites.* Figure 5 displays the effective dispersion of NH_2-NMS, as revealed by the transmission electron microscopy of a cross section of polyimide nanocomposites. Even in the sample with 10 wt % NMS, NMS nanoparticles are well dispersed in the film as shown in Figure 5C. The inorganic phase does not easily disperse in most polyimide nanocomposites with 10 wt % of inorganic compound. An additional TEM image, which is 4 times the area shown in Figure 5C, also shows well dispersion of NMS in polyimide matrix in the Supporting Information. Covalent bonding between the polyimide main chain and the amino group on the surface inside the channel is important in the effective dispersion of NMS in the polyimide matrix. NMS nanoparticles in composites are irregularly shaped, and their sizes are similar to those of blank NMS, while the particle size distribution seems uneven because of the cross section of the composite film prepared from microtome. The bright pore image for the NMS in composites can be still observed in Figure 5B, but the contrast between the silica wall and the pore becomes ambiguous because the pore is no longer empty and a polymer chain exists inside

Table 1. Physical Properties of Various Nanoscaled Mesoporous Silica Materials

sample	d_{100} (nm)	D_p[a] (nm)	V_t[b] (cm^3/g)	S_{BET}[c] (m^2/g)	elemental analysis (%) C	H	N
NMS	3.55	2.71	1.16	944	0	0	0
NH_2-NMS		<1.7	0.59	275	8.5	2.0	2.9
ODPA-NH_2-NMS		<1.7	0.21	93	14.2	2.2	2.7

[a] Pore diameter. [b] Total pore volume calculated from $P/P_0 = 0.99$. [c] BET surface area.

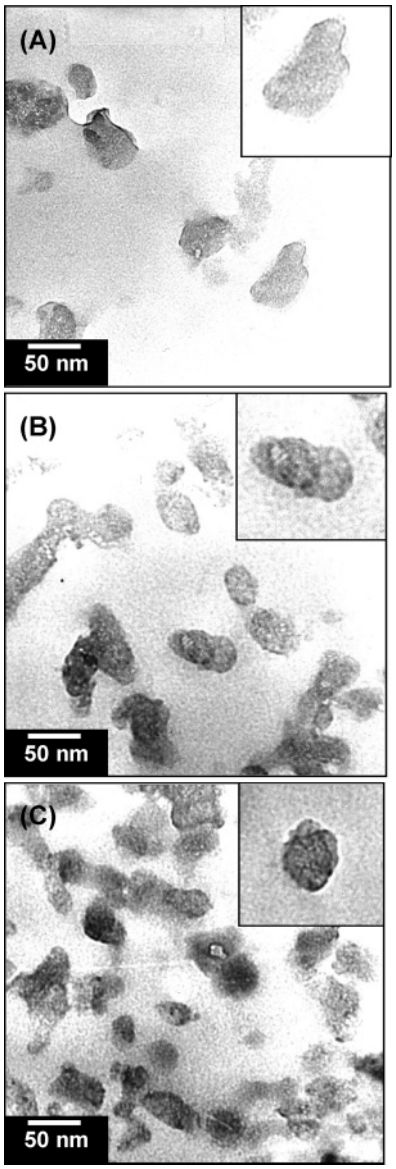

Figure 5. TEM images of the polyimide nanocomposites with various NH_2-NMS loadings: (A) 1, (B) 3, and (C) 10 wt %. Enlarged NMS is shown in the inset.

the channel. This evidence also demonstrates the anchor and the blockage of the polymer main chain inside the pore channel.

Thermogravimetric Analysis (TGA). Figure 6 and Table 2 present the thermal stabilities of polyimide nanocomposites tethered NMS, investigated by TGA. All systems show better thermal stability than the neat polyimide. The thermal degradation temperatures of nanocomposites increase with the amount of NH_2-NMS. The onset decomposition temperature (T_d) of nanocomposite with 3 wt % NMS increases from 521.2 °C (neat polyimide) to 529.7 °C. Further increasing NMS loading to 10 wt % yields, the T_d of the nanocomposite is 556.9 °C, representing an increase of 35.7 °C. One NMS nanoparticle has abundant silanol groups on the particle surface and internal pore

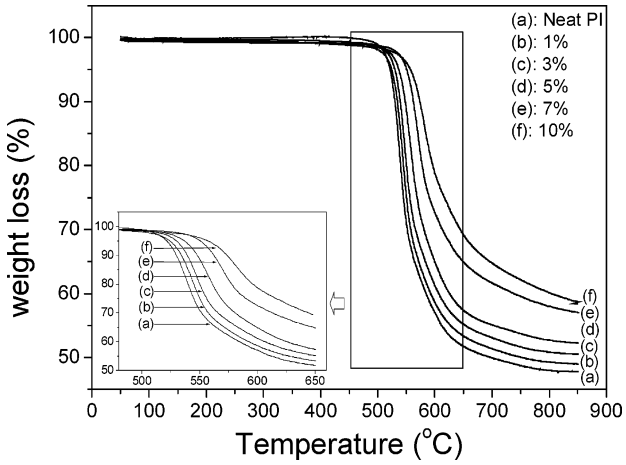

Figure 6. TGA curves of the neat polyimide and polyimide nanocomposites with various NH_2-NMS loadings.

channel surface, which can form covalent bonds with the polymer monomers via the APTMS silane bridge. Polyimide polymer chains not only bond to the surface of the NMS particle but also penetrate the pore channel and are tethered the channel surface. The char yield of NMS/PI increases with the NMS weight percentage, probably because PI main chains on NMS surface and inside NMS pore are more difficult to decompose than the neat one. Therefore, the improvement in thermal stability of NMS/PI is ascribed to both the good thermal stability of NMS and the multilinkage between the polyimide chain and NMS with multiamino groups.

Differential Scanning Calorimetry (DSC). Figure 7 presents DSC traces of polyimide nanocomposites with different compositions. Neat polyimide exhibits an endotherm at 224.6 °C, corresponding to the glass transition temperature of pure polyimide. The glass transition temperatures (T_g) of NMS/PI nanocomposites increase slightly with the amount of modified NMS. The polyimide with 10 wt % NH_2−NMS has a T_g of up to 14.5 °C higher than that of neat polyimide. The increase in the glass-transition temperature of the polyimide nanocomposites may be caused by the two following factors. The "pseudo-molecular weight" of the polyimide is higher in the NMS/PI nanocomposites because of multilinkage between the PAA main chains and the silanol group NMS on the surface of the particles or the pore channels via the APTMS bridge. Multilinkage between the polyimide main chain and NH_2-NMS may retard the motion of poyimide main chain.

Dynamic Mechanical Analyses (DMA). Table 2 and Figure 8 show the results of dynamic mechanical analyses (DMA) and the corresponding glass-transition temperatures of the NMS/PI nanocomposites with various NMS loadings. These polyimide nanocomposites have a higher storage modulus and T_g than neat polyimide. The storage modulus of the NMS/PI nanocomposites increases from 1.8 to 4.8 GPa at 45 °C as the amount of modified NMS increases from 0 to 10 wt %. The storage modulus of the polyimide nanocomposite with 10 wt % NH_2-NMS is 2.6 times that of pristine polyimide. As shown in Figure 8B, the tan δ peaks of each nanocomposite apparently shift to

Table 2. Thermal, Mechanical, and Other Properties of NMS/PI Nanocomposites with Different NMS Amounts

amount of NH_2-NMS	T_d[a] (°C)	T_g[b] (°C)	T_g[c] (°C)	storage modulus (GPa)	max stress (MPa)	max elongation (%)	dielectric constant (at 1 Mz)	water uptake (wt %)
neat PI	521.2	224.6	233.1	1.8	84.9	7.6	3.46 ± 0.02	2.97
1%	524.1	225.8	235.2	2.1	93.5	8.2	3.35 ± 0.01	2.54
3%	529.7	229.6	237.0	2.6	104.1	10.6	3.27 ± 0.01	2.36
5%	536.5	231.6	241.7	3.8	111.9	11.4	3.19 ± 0.03	2.19
7%	550.5	235.1	244.6	4.2	116.7	12.1	3.13 ± 0.01	2.10
10%	556.9	239.3	247.9	4.8	123.6	12.6	3.11 ± 0.02	1.97

[a] Decomposed temperature at 5% weight loss. [b] Glass-transition temperatures by DSC. [c] Glass-transition temperatures by DMA.

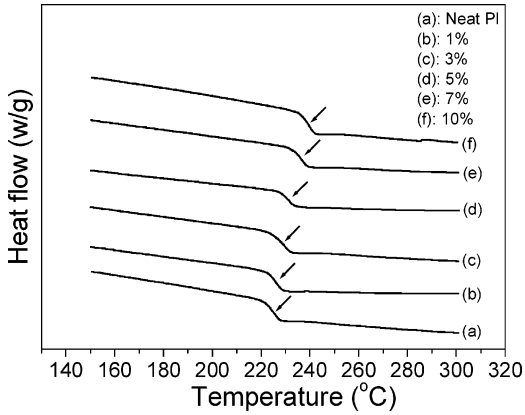

Figure 7. DSC curves of the neat polyimide and polyimide nanocomposites with various NH_2-NMS loadings.

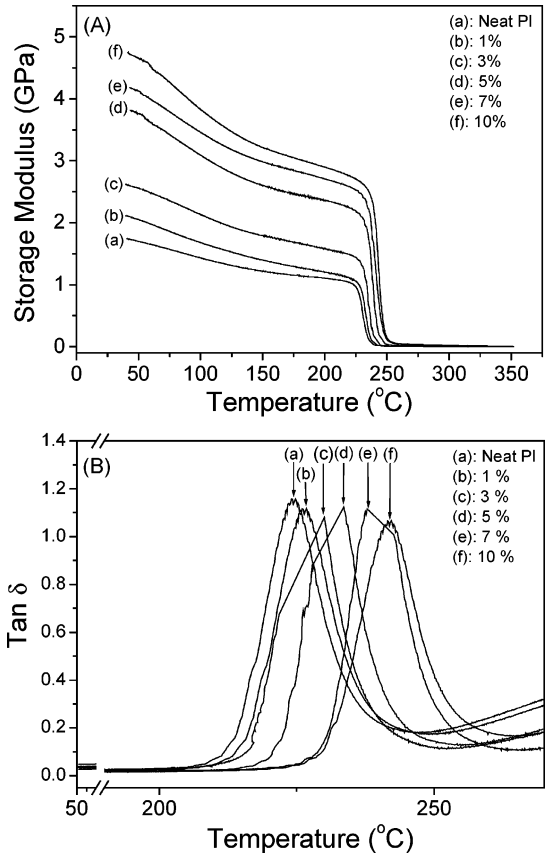

Figure 8. Relationship between (A) the storage modulus and (B) tan δ and temperature as obtained from DMA measurements on the membranes of neat polyimide and polyimide nanocomposites with various NH_2-NMS loadings.

higher temperatures. The largest increase in the T_g of 10 wt % polyimide nanocomposites over that of the neat polyimide is 14.8 °C. The T_g of the polyimide nanocomposites measured by DMA slightly exceeds that determined by DSC, but the

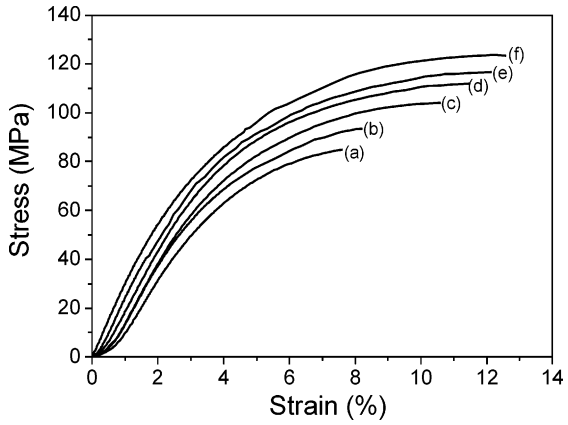

Figure 9. Typical stress−strain curves of the neat polyimide and polyimide nanocomposites with different NH_2-NMS loadings.

dependency of the transition temperature on the amount of NH_2-NMS is consistently revealed by both sets of data. The improvement in the dynamic thermomechanical characteristics of NMS/PI is caused by the following. Numerous polyimide main chains can anchor on the particle and the pore channel surface of a single NMS. The enhanced mechanical properties of the polymer network follow frrom the rigidity of inorganic NMS, the high "pseudo-molecular weight" and dense linkage between the carboxylic groups of poly(amic acid) and the amino groups of NH_2-NMS. The rigidity and multilinkage of NH_2-NMS with polyimide also effectively constrains the polyimide main-chain motion, thus increasing the T_g of the composite.

Mechanical Properties. Figure 9 plots typical stress−strain curves of the pure polyimide and NMS/PI nanocomposites. The maximum stress of the polyimide nanocomposites increases from 84.9 (neat polyimide) to 123.6 MPa at 45 °C as the amount of NMS materials is increased from 0 to 10 wt %. When the amount of NMS materials in polyimide is 10 wt %, the maximum stress of the polyimide nanocomposites is 46% greater than that of the pure polyimide. The continuous increase in maximum stresses of these nanocomposites with the amount of NMS amount suggests that the interfacial strength between NH_2-NMS and polyimide exceeds that between polyimide molecules. This result may follow from the effective covalent bond through the pore channel and the homogeneous dispersion of NMS in the polyimide matrix. The homogeneous dispersion of NMS in the polyimide was confirmed by TEM image as shown in Figure 5. The elongation of polyimide nanocomposites increases strongly with the amount of NH_2-NMS materials to a maximum of 66% more than that of neat polyimide. Most PI/silica, PI/clay, and PI/POSS[30,43] nanocomposites with high inorganic contents[39,40] may display higher tensile strength, but most composites display lower elongation and become more fragile than neat polyimide. The bonding between the polymer and the inorganic moiety may be not as strong as the intrapolymer bonds. Hence, most nanocomposites are more fragile than neat polyimide. The following two causes are probably respon-

Scheme 2. Model of NMS/PI Nanocomposite Matrix

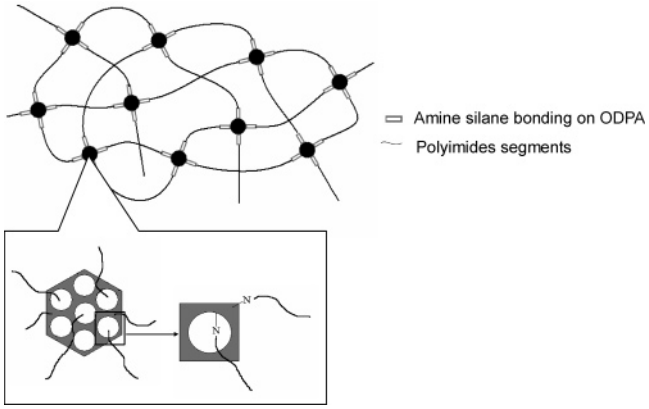

sible for the higher maximum elongation and elasticity of NMS/PI composites than that of neat polyimide. First, polyimide chains not only covalently bond with the reactive channel functional groups of NMS but also interact via the van der Waals forces with the channel surface molecules because the polymer intrudes into NMS nanopores. Second, pore space of NMS in polyimide composite can absorb more energy than that in pristine polyimide before failure.[44]

Water Absorption. The water absorption of polyimides applied to microelectronic devices enhances the dielectric constant of polyimide and promotes the corrosion of metal conductors in devices. Therefore, a polyimide with low water uptake is urgently necessary for high-level microelectronic devices. The water uptake of the NMS/PI declines from 2.97 to 1.97% as the NMS amount increases from 0 to 10%. The substantial reduction of water uptake for these nanocomposites is probably associated with the increase in hydrophobicity caused by the adding of NMS via covalent bonding.

Dielectric Properties. A lower dielectric constant is one of the most desirable properties for the next generation of electronic devices. The dielectric constant of polyimide nanocomposites was measured using a dielectric analyzer (DEA). Table 2 gives the dielectric constants of various polyimide nanocomposites with various NH_2-NMS contents. The polyimide nanocomposites with added NH_2-NMS have lower dielectric constants than neat polyimide. The dielectric constant of the neat polyimide is 3.46, while the lowest dielectric constant of the polyimide nanocomposites with 10 wt % NMS is 3.11. The reduction of the dielectric constant depends on the amount of NH_2-NMS material in the polyimide nanocomposites because of the nanoporosity of the core of the NH_2-NMS material as shown in Figure 5. Part of NMS nanopores may fill with polymer or other oligomers, but some of the nanoporous space is available, as evidenced by the drop in film density.

Conclusions

Novel nanoscale mesoporous silica/polyimide nanocomposites were synthesized via covalent bonding between NMS and polyimide. The inorganic moiety of the nanocomposite, which is nanoscale mesoporous silica with a size of around 60 nm size, is not only nanoscale silica but also has many nanopores in its interior. Scheme 2 gives the model of the NMS/PI nanocomposite matrix. One NMS nanoparticle has abundant silanol groups on its particle surface and on the surface of its internal pore channel, which can form covalent bonds with polymer main chains via the APTMS silane bridge. Polymer chains not only bond to the NMS particle surface but also penetrate the pore channel, becoming tethered to the channel surface. Hence, the NMS-reinforced polymer network is formed by the rigidity of inorganic NMS, its high "pseudo-molecular weight", and the multilinkage between the carboxylic groups of poly(amic acid) and the amino groups of NH_2-NMS. The rigidity and multilinkage of NH_2-NMS with polyimide can also effectively constrain the motion of the polyimide main chain, improving the T_g of the composite. Most nanocomposites prepared by the sol−gel method, intercalation, physical blending, and the tethering of POSS are brittle, but the NMS/PI matrix has much better maximum elongation than those above-mentioned nanocomposites. The dielectric constants of these materials are 10% lower than that of neat polyimide. The nanoporosity of the core of the NH_2-NMS material in the nanocomposite film must be important in improving these characteristics.

Acknowledgment. The authors thank the National Science Council of the Republic of China for financially supporting this research under Contracts NSC94-2113-M-033-006 and NSC94-2745-M-033-003-urd. The Center-of-Excellence Program on Membrane Technology, the Ministry of Education, Taiwan, R.O.C., is also appreciated.

Supporting Information Available: TEM image of the polyimide nanocomposites with 10 wt % NH_2-NMS loadings. This material is available free of charge via the Internet at http://pubs.acs.org.

References and Notes

(1) Klok, H. A.; Lecommandoux, S. *Adv. Mater.* **2001**, *13*, 1217.
(2) Sanchez, C.; Soler-Illia, G. J. de A. A.; Ribot, F.; Lalot, T.; Mayer, C. R.; Cabuil, V. *Chem. Mater.* **2001**, *13*, 3061.
(3) Sharp, K. G. *Adv. Mater.* **1998**, *10*, 1243.
(4) Zhu, Z.; Yang, Y.; Yin, J.; Qi, Z. *J. Appl. Polym. Sci.* **1999**, *73*, 2977.
(5) Adadie, M. J. M.; Sillion, B. In *Polyimides and Other High-Temperature Polymers*; Elsevier: Amsterdam, 1991.
(6) Feger, C.; Khojasteh, M. M.; McGrath, J. E. In *Polyimides: Chemistry and Characterization*; Elsevier: Amsterdam, 1994.
(7) Wilson, D.; Stenzenberger, H. D.; Hergenrother, P. M. In *Polyimides*; Black & Son: Glasgow, 1990.
(8) Chen, Y.; Iroh, J. O. *Chem. Mater.* **1999**, *11*, 1218.
(9) Agag, T.; Koga, T.; Takeichi, T. *Polymer* **2001**, *42*, 3399.
(10) Xenopoulos, C.; Mascia, L.; Shaw, S. J. *J. Mater. Chem.* **2002**, *12*, 213.
(11) Chang, C. C.; Chen, W. C. *Chem. Mater.* **2002**, *14*, 4242.
(12) Hedrick, J. L.; Cha, H. J.; Miller, R. D.; Yoon, D. Y.; Brown, H. R.; Srinivasan, S.; Cook, R. F.; Hummel, J. P.; Klaus, D. P.; Liniger, E. G.; Simonyi, E. E. *Macromolecules* **1997**, *30*, 8512.
(13) Srinivasan, S. A.; Hedrick, J. L.; Miller, R. D. *Polymer* **1997**, *38*, 3129.
(14) Ahmad, Z.; Mark, J. E. *Chem. Mater.* **2001**, *13*, 3320.
(15) Tsai, M. H.; Whang, W. T. *Polymer* **2001**, *42*, 4197.
(16) Cornelius, C. J.; Marand, E. *Polymer* **2002**, *43*, 2385.
(17) Shang, X. Y.; Zhu, Z. K.; Yin, J.; Ma, X. D. *Chem. Mater.* **2002**, *14*, 71.
(18) Wen, J.; Wilkes, G. L. *Chem. Mater.* **1996**, *8*, 1667.
(19) Chen, W. C.; Lee, S. J.; Lee, L. H.; Lin, J. L. *J. Mater. Chem.* **1999**, *9*, 2999.
(20) Kim, Y.; Kang, E.; Kwon, Y. S.; Cho, W. J.; Cho, C.; Chang, M.; Ree, M.; Cang, T.; Ha, C. S. *Synth. Met.* **1997**, *85*, 1399.
(21) Kim, Y.; Lee, W. K.; Cho, W. J.; Ha, C. S. *Polym. Int.* **1997**, *43*, 129.
(22) Choi, J.; Tamaki, R.; Kim, S. G.; Laine, R. M. *Chem. Mater.* **2003**, *15*, 3365.
(23) Lee, Y. J.; Huang, J. M.; Kuo, S. W.; Chang, F. C. *Polymer* **2005**, *46*, 10056.
(24) Huang, J. C.; He, C. B.; Liu, X. M.; Xu, J. W.; Tay, C. S. S.; Chow, S. Y. *Polymer* **2005**, *46*, 7018.
(25) Lee, Y. J.; Huang, J. M.; Kuo, S. W.; Lu, J. S.; Chang, F. C. *Polymer* **2005**, *46*, 173.
(26) Huang, J. C.; Xiao, Y.; Mya, K. Y.; Liu, X. M.; He, C. B.; Dai, J.; Siow, Y. P. *J. Mater. Chem.* **2004**, *14*, 2858.
(27) Leu, C. M.; Reddy, G. M.; Wei, K. H.; Shu, C. F. *Chem. Mater.* **2003**, *15*, 2261.
(28) Leu, C. M.; Chang, Y. T.; Wei, K. H. *Chem. Mater.* **2003**, *15*, 3721.
(29) Leu, C. M.; Chang, Y. T.; Wei, K. H. *Macromolecules* **2003**, *36*, 9122.

(30) Huang, J. C.; He, C. B.; Xiao, Y.; Mya, K. Y.; Dai, J.; Siow, Y. P. *Polymer* **2003**, *44*, 4491.
(31) Huang, J. C.; He, C. B.; Liu, X. M.; Xu, J. W.; Tay, C. S. S.; Chow, S. Y. *Polymer* **2005**, *46*, 7018.
(32) Huang, J. C.; Lim, P. C.; Shen, L.; Pallathadka, P. K.; Zeng, K. Y.; He, C. B *Acta Mater.* **2005**, *53*, 2395.
(33) Choi, J.; Yee, A. F.; Laine, R. M. *Macromolecules* **2003**, *36*, 5666.
(34) Tsai, M. H.; Whang, W. T. *Polymer* **2001**, *42*, 4197.
(35) Nooney, R. I.; Thirunavukkarasu, D.; Chen, Y. M.; Josephs, R.; Ostafin, A. E. *Chem. Mater.* **2002**, *14*, 4721.
(36) Fowler, C. E.; Khushalani, D.; Lebeau, B.; Mann, S. *Adv. Mater.* **2001**, *13*, 649.
(37) Cheng, C. F.; Cheng, H. H.; Wu, L. L.; Cheng, B. W. *Stud. Surf. Sci. Catal.: Nanoporous Mater.* **2005**, *156*, 113.
(38) Blin, J. L.; Gèrardin, C.; Rodehüser, L.; Selve, C.; Stèbè, M. J. *Chem. Mater.* **2004**, *16*, 5071.
(39) Musto, P.; Ragosta, G.; Scarinzi, G.; Mascia, L. *Polymer* **2004**, *45*, 1697.
(40) Chen, B. K.; Chiu, T. M.; Tsay, S. Y. *J. Appl. Polym. Sci.* **2004**, *94*, 382.
(41) Wang, H. W.; Dong, R. X.; Chu, H. C.; Chang, C. K.; Lee, W. C. *Mater. Chem. Phys.* **2005**, *94*, 42.
(42) Zhang, Y. H.; Wu, J. T.; Fu, S. Y.; Yang, S. Y.; Li, Y.; Fan, L.; Li, R. K. Y.; Li, L. F.; Yan, Q. *Polymer* **2004**, *45*, 7579.
(43) Huang, J.; Lim, P. C.; Shen, L.; Pallathadka, P. K.; Zeng, K.; He, C. *Acta Mater.* **2005**, *53*, 2395.
(44) Rodriguez, F.; Cohen, C.; Ober, C.; Archer, L. A. In *Principles of Polymer Systems*, 5th ed.; London: New York, 2003.

MA060990U